Published in final edited form as:
Nonlinear Dyn. 2010 October 1; 62(1): 291–303. doi:10.1007/s11071-010-9717-3.

Minimal formulation of joint motion for biomechanisms

Ajay Seth, **Michael Sherman**, **Peter Eastman**, and **Scott Delp**
Bioengineering Department, Stanford University, Stanford, CA 94305-5448, USA

Abstract

Biomechanical systems share many properties with mechanically engineered systems, and researchers have successfully employed mechanical engineering simulation software to investigate the mechanical behavior of diverse biological mechanisms, ranging from biomolecules to human joints. Unlike their man-made counterparts, however, biomechanisms rarely exhibit the simple, uncoupled, pure-axial motion that is engineered into mechanical joints such as sliders, pins, and ball-and-socket joints. Current mechanical modeling software based on internal-coordinate multibody dynamics can formulate engineered joints directly in minimal coordinates, but requires additional coordinates restricted by constraints to model more complex motions. This approach can be inefficient, inaccurate, and difficult for biomechanists to customize. Since complex motion is the rule rather than the exception in biomechanisms, the benefits of minimal coordinate modeling are not fully realized in biomedical research. Here we introduce a practical implementation for empirically-defined internal-coordinate joints, which we call “mobilizers.” A mobilizer encapsulates the observations, measurement frame, and modeling requirements into a hinge specification of the permissible-motion manifold for a minimal set of internal coordinates. Mobilizers support nonlinear mappings that are mathematically equivalent to constraint manifolds but have the advantages of fewer coordinates, no constraints, and exact representation of the biomechanical motion-space—the benefits long enjoyed for internal-coordinate models of mechanical joints. Hinge matrices within the mobilizer are easily specified by user-supplied functions, and provide a direct means of mapping permissible motion derived from empirical data. We present computational results showing substantial performance and accuracy gains for mobilizers versus equivalent joints implemented with constraints. Examples of mobilizers for joints from human biomechanics and molecular dynamics are given. All methods and examples were implemented in Simbody™—an open source multibody-dynamics solver available at https://Simtk.org.

Keywords

Multibody dynamics; Internal coordinates; Computer simulation; Biomechanics; Molecular dynamics; Skeletal modeling

1 Introduction

Physics-based simulations of biological structures employ computational tools to understand the dynamics of complex biological mechanisms that influence human health. Simulations of musculoskeletal dynamics, for example, are used to quantify joint reaction forces of articulating bones in studies of osteoarthritis [1,2] and joint prosthetics [3]. Simulations of molecular machines [4-6] are used to characterize the dynamics of molecular processes in biology. To gain confidence in biosimulations, models must be accurate and subjected to

aseth@stanford.edu, http://www.stanford.edu/group/nmbl/.

sensitivity [7] and design optimization [8] analyses, demanding vast amounts of computation. Simulation accuracy and efficiency are generally competing goals, but here we present a multibody formulation that improves both, and is well-suited for, simulation of biomechanisms.

Structures over a wide range of biological domains can be modeled as systems of rigid bodies connected by joints; that is, multibody systems. Although force calculations and specialized numerical methods [9] affect the cost of simulating biomechanisms, our focus is on the efficiency of the multibody dynamics formulation. The multibody dynamics formulation influences the number of force calculations and the demands on numerical methods. We consider internal coordinate formulations [10], implemented using an O(n) recursive algorithm (surveyed by Jain [11]), to be the preferred method for simulating biomechanisms. Internal coordinates are particularly useful because coordinates are directly related to degrees of freedom (dofs) of interest. Internal coordinates also provide a minimal set of system equations with the opportunity to obtain a system free of algebraic constraints, which yields a system composed of ordinary differential equations (ODEs) and avoids numerically intensive mixed differential algebraic equations (DAEs) [12]. A system of ODEs does not require constraint stabilization [13,14] and is better suited for design optimization [15,16] and sensitivity analyses [17], as well as optimal control [18,19] applications. Internal coordinate formulations are prevalent in musculoskeletal modeling [20-23] and ubiquitous in coarse-grained biomolecular dynamics for NMR refinement [24-26]. In other biomolecular contexts, multibody dynamics has yet to be fully exploited, but internal-coordinate methods have already been applied successfully [27-29]. For mechanically engineered systems, limitations resulting from the underlying tree structure and the complexity of recursive internal coordinate formulations have been successfully resolved (e.g. [30-32]); addressing the challenges for efficiently representing biomechanisms is the subject of this paper.

To illustrate one of the challenges with a simplified example, consider the representation of screw motion that has a single rotation about a screw axis and a translation along the same axis (z-axis, Fig. 1), which are coupled by the screw's pitch s (in m/rad, for example). Whereas typical mechanical joints such as a pin, slider, universal, cylindrical, and planar partition motion into rotational and translational components, a screw joint inconveniently couples a rotation and a translation. In automated software having no built-in screw, a common approach [33,34] is to employ a cylindrical joint providing two dofs with internal coordinates u_1 and u_2 and then to enforce the relationship of rotation to translation via the constraint $u_2 = su_1$. The result is a set of three DAEs (one rotational and one translational differential equation, and one algebraic equation). While this is a substantial reduction from the eleven equations required by spatial formulations (three rotational and three translational differential equations, and five algebraic equations), it still requires a system of three DAEs to model a single dof.

In practice, of course, a screw can be treated efficiently [45]. But the problem is more severe for biomechanical joints, where a knee [35] or shoulder [36] couples multiple rotational and translational motions according to bone geometry that differs between subjects and must be determined empirically. Coarse-grained models of biomolecular machines can also lead to coupled, empirically described motion [37]. Lee and Terzopoulos [38] recognized this limitation of mechanical joints and introduced a spline joint in a differential geometry framework for expressing a complex motion path in terms of a single internal coordinate.

In this paper we introduce a practical, extensible formulation and implementation of the internal-coordinate joint, called a "mobilizer," which encapsulates a general mapping of complex joint motion, including motion that is empirically-determined, to internal

coordinates critical for modeling biomechanisms, and deals with pragmatic issues such as the laboratory frame and joint directionality (from parent to child) associated with the spanning-tree structure of internal-coordinate methods. We begin with the mobilizer formulation and demonstrate how to define the screw above and a novel ellipsoid joint with a mobilizer. These examples lead to the derivation of a user-configurable mobilizer, which we use to define a realistic biomechanical knee model and a coarse-grained molecular model. We compare the performance of mobilizers to conventional joints using constraints and discuss the implications of mobilizers for the simulation of biomechanisms.

2 Joints in internal coordinates

In biomechanics the term “joint” connotes a physically-realizable connection that can be represented by various combinations of coordinates and algebraic constraints. The term “hinge” refers to a revolute rotational joint. To avoid confusion between these physical objects, the multibody dynamics concepts of the generalized hinge, and their computational representations, we use the term “mobilizer” to encapsulate the complete specification of the unconstrained motion permitted between two bodies, modeling requirements, and the resulting implementation in software. A single mobilizer connects each body of a multibody system to its unique “parent” body forming a tree topology; that concept is often called a “hinge” in internal-coordinate multibody dynamics literature (e.g. [39]). A body connected by a mobilizer introduces new coordinates q and speeds u to the system, which we term “mobilities,” but does not add constraints. This contrasts the conventional notion that every rigid body has six dofs, some of which may be *removed* by joints. We take the view that a body only possesses those dofs that are *granted* by its mobilizer. This provides a clear distinction between a body connected by a pin mobilizer (i.e. the internal-coordinate joint representation) introducing a single mobility and an ODE, and an otherwise free (6-dof) rigid body constrained by a pin (five algebraic constraints) that leads to a set of 11 DAEs.

2.1 Mobilizer representation of permissible motion

The main purpose of a mobilizer is to define the permissible-motion space spanned only by coordinates that are degrees of freedom associated with a physical joint. To do so, we build on the internal-coordinate concept of the “hinge matrix” [39] (also “hinge map matrix” [31]; “joint map matrix” [40]; or “joint motion map matrix” [25,41]), which is a mapping between mobilities and the relative spatial kinematics used to formulate the recursive Newton–Euler equations of motion [42]. Specifically, we exploit the hinge matrix and its time derivative to map the permissible-motion space of a physical joint, in terms of the mobilities that correspond to joint dofs, which would otherwise require scleronomic constraints acting on spatial kinematics.

The Internal Variable Dynamics Module (IVM) of X-PLOR [25] was built on internal-coordinate methods using spatial operators described by Jain et al. [39], and we have built on this fundamental framework to implement the mobilizer and develop the multipurpose open-source multibody dynamics solver, Simbody, as part of a biosimulation toolkit (SimTK [43], https://simtk.org).

In Simbody, a mobilizer from parent frame P to child frame B is completely characterized by the following four equations:

$$ {}^{P}\mathbf{X}^{B} \equiv \left[{}^{P}\mathbf{R}^{B}(q) \quad {}^{P}p^{B}(q) \right], \tag{1} $$

$$ {}^{P}V^{B} \equiv \left\{ \begin{array}{c} {}^{P}\omega^{B}(q,u) \\ {}^{P}v^{B}(q,u) \end{array} \right\} = {}^{P}\mathbf{H}^{B}(q) \cdot u, \tag{2} $$

$$ {}^{P}A^{B} \equiv {}^{P}\dot{V}^{B} = {}^{P}\mathbf{H}^{B}\,\dot{u} + {}^{P}\dot{\mathbf{H}}^{B}\,u, \tag{3} $$

$$ \dot{q} = \mathbf{N}(q)\,u. \tag{4} $$

Equation (1) describes the position transform, ${}^{P}\mathbf{X}^{B}$, comprised of the rotation matrix, **R**, and translation vector, *p*, of a mobilizer frame, *B*, fixed in the body (B_o frame) with respect to a parent mobilizer frame *P*, fixed in the parent body (P_o) (Fig. 2). The spatial velocity, ${}^{P}V^{B}$ in (2), and acceleration, ${}^{P}A^{B}$ in (3), of *B* with respect to *P*, are specified by the hinge matrix, **H**, and its time derivative, $\dot{\mathbf{H}}$. The evolution of the coordinates, *q*, is governed by the differential relationship (4) with the mobilities, *u*, according to the kinematic coupling matrix **N**. Each of these elements can be found in the literature; our contribution is to present them in a form which permits non-dynamicist end users to routinely map external data into novel internal-coordinate joints, as will be shown below.

In formulations where explicit constraints are used, joint reaction forces are obtained directly from the Lagrange multipliers used to enforce the constraints [44]. However, explicit constraints are unnecessary to compute reaction loads (e.g. bearing loads of a pin joint) and can be obtained from the spatial accelerations of the bodies from (3). Internal-coordinate codes like SD/FAST [33] and Simbody use a recursive force balance from leaf bodies inwards to the root to yield the reactions imposed by each mobilizer.

2.2 Screw mobilizer example

In the screw motion example (Fig. 1), either the angular (u_1) or the translational speed (u_2) of the collar (blue) with respect to the screw (green) is a good choice for the mobility. Given the pitch *s* of the screw, we choose the angular speed of the collar as the single mobility, *u*, and its angular position as the single coordinate, *q*, such that $\dot{q} = u$. The mobilizer equations for the collar (the child) body with respect to a frame fixed in the screw (the parent) are:

$$ {}^{P}\mathbf{X}^{B} = \begin{bmatrix} \cos(q) & -\sin(q) & 0 & 0 \\ \sin(q) & \cos(q) & 0 & 0 \\ 0 & 0 & 1 & sq \end{bmatrix}, \tag{5} $$

$$ {}^{P}V^{B} = \begin{bmatrix} 0 & 0 & 1 & 0 & 0 & s \end{bmatrix}^{\mathrm{T}} u, \tag{6} $$

$$ {}^{P}A^{B} = \begin{bmatrix} 0 & 0 & 1 & 0 & 0 & s \end{bmatrix}^{\mathrm{T}} \dot{u}, \tag{7} $$

such that ${}^{P}\mathbf{H}^{B} = \begin{bmatrix} 0 & 0 & 1 & 0 & 0 & s \end{bmatrix}^{\mathrm{T}}$ and ${}^{P}\dot{\mathbf{H}}^{B} = 0$.

The hinge matrix, **H**, effectively describes mechanical joints, and has been used elsewhere to model the coupled motion of the screw joint using a single internal coordinate (e.g. [30,45]). We now extend this capability to capture more complex permissible-motion granted by a mobilizer to specify the behavior of biomechanical joints. The mobilizer mapping equations (1)–(3) enable the modeler to specify the transformation between

arbitrary mobilizer frames on the parent and body (*P* and *B*,Fig. 2) that may be dictated by the data collection apparatus, or otherwise preferred as more natural descriptions of joint motions than transformations described with respect to body origins or mass centers. Multibody formulations based on mechanical joints (including composites of pins and sliders) are typically written in terms of body frames, and are limited to coordinate choices that yield a constant **H** [39] or specifically map from angular parameterizations (e.g. Euler angles and speeds) to relative angular velocity [25,46]. Simbody enables user-selected frames and a general form for **H** and its derivative to permit users to create novel and biologically accurate mobilizers.

2.3 Ellipsoid mobilizer example

Several biologically inspired joints highlight the variety of permissible-motion manifolds realizable by the mobilizer formulation. The ellipsoid mobilizer extends the ball-and-socket joint to enable translation of the body such that it is bound to the surface of an ellipsoid (fixed in the parent) as the body rotates about the parent. Unlike a ball-and-socket joint, an ellipsoid joint would be difficult to manufacture and few industrial machines employ one; however, in nature similar joints exist. Specifically, in human biomechanics, the hip joint has been reported to be more ellipsoidal in shape [47] than a pure ball-and-socket, and Van der Helm et al. [36] have described the thorax as an ellipsoid upon which the scapula (shoulder blade) translates and rotates (Fig. 3).

We begin with the formulation of the conventional ball-and-socket mobilizer (Fig. 4A):

$$ {}^{P}\mathbf{X}^{B} = \begin{bmatrix} {}^{P}\mathbf{R}^{B}(q) & 0 \end{bmatrix} \tag{8} $$

where $q = \{\theta_1, \theta_2, \theta_3\}$ is a body-fixed 1–2–3 Euler sequence of rotations (assuming a limited range of rotation). The spatial velocity is specified by the hinge matrix:

$$ {}^{P}\mathbf{H}^{B} = \begin{bmatrix} 1 & 0 & 0 & 0 & 0 & 0 \\ 0 & 1 & 0 & 0 & 0 & 0 \\ 0 & 0 & 1 & 0 & 0 & 0 \end{bmatrix}^{\mathrm{T}}, \tag{9} $$

where the chosen mobilities $u = [\omega_1\ \omega_2\ \omega_3]^{\mathrm{T}}$ are the components of the angular velocity vector of *B* in *P* (Fig. 2). Typical of mechanical joints, ${}^{P}\dot{\mathbf{H}}^{B} = 0$ for the ball-and-socket mobilizer, but the kinematic coupling matrix $\mathbf{N} \neq \mathbf{I}$ in (4) and maps from angular velocity to Euler angle derivatives [10]:

$$ \mathbf{N}(q) = \begin{bmatrix} \cos\theta_3/\cos\theta_2 & -\sin\theta_3/\cos\theta_2 & 0 \\ \sin\theta_3 & \cos\theta_3 & 0 \\ -\sin\theta_2\cos\theta_3/\cos\theta_2 & \sin\theta_2\sin\theta_3/\cos\theta_2 & 1 \end{bmatrix}. \tag{10} $$

The ellipsoid mobilizer (Fig. 4B) has the same angular definition as the ball-and-socket, but rather than grant 3 additional mobilities for spatial translations, which would then have to be constrained, the translations are coupled to the orientation of the body such that:

$$ {}^{P}\mathbf{X}^{B} = \begin{bmatrix} {}^{P}\mathbf{R}^{B}(q) & p(q) \end{bmatrix}, \tag{11} $$

where *q* remains the 1–2–3 Euler angle sequence describing the orientation of the body, but now

$$p(q) = \begin{Bmatrix} an_1 \\ bn_2 \\ cn_3 \end{Bmatrix} = \begin{Bmatrix} a\sin(\theta_2) \\ b(-\sin(\theta_1)\cos(\theta_2)) \\ c\cos(\theta_1)\cos(\theta_2) \end{Bmatrix} \tag{12}$$

describes the translation of the body's mobilizer frame, *B*, onto the surface of an ellipsoid ($n = n(q)$ being the normal vector) fixed in the parent's mobilizer frame, *P*, with *a*, *b*, *c* corresponding to the ellipsoid radii along the axes of *P*. The angular velocity remains the same function of *u* as for the ball-and-socket joint, so **N** is unchanged from (10), but now there are coupled linear velocities that are a consequence of the rotating normal vector; this results in the ellipsoid hinge matrix having the form:

$${}^{P}\mathbf{H}^{B} = \begin{bmatrix} 1 & 0 & 0 & 0 & -bn_3 & cn_2 \\ 0 & 1 & 0 & an_3 & 0 & -cn_1 \\ 0 & 0 & 1 & -an_2 & bn_1 & 0 \end{bmatrix}^{\mathrm{T}}. \tag{13}$$

In this case, $\dot{\mathbf{H}} \neq 0$ and must be resolved to obtain angular velocity contributions to the body's linear acceleration:

$${}^{P}\dot{\mathbf{H}}^{B} = \begin{bmatrix} 0 & 0 & 0 & 0 & -b\dot{n}_3 & c\dot{n}_2 \\ 0 & 0 & 0 & a\dot{n}_3 & 0 & -c\dot{n}_1 \\ 0 & 0 & 0 & -a\dot{n}_2 & b\dot{n}_1 & 0 \end{bmatrix}^{\mathrm{T}}. \tag{14}$$

The hinge matrix ${}^{P}\mathbf{H}^{B}$ and its derivative ${}^{P}\dot{\mathbf{H}}^{B}$ span exactly and map only onto the subspace of the permissible-motion manifold of an ellipsoid surface. If limited to multibody dynamics codes with conventional joints, then a free joint (six dofs) is required with an additional three constraint equations, for a total of nine DAEs versus the mobilizer formulation's three ODEs.

We compared the ellipsoid mobilizer to a ball-and-socket mobilizer and an ellipsoid joint implementation with nine DAEs (Table 1). The ellipsoid mobilizer formulation had the same computational cost as a ball-and-socket mobilizer in terms of evaluating the system acceleration and reaction loads for a given configuration as well as for integrating the equations of motion in a simulation. We expected computation of the system acceleration and reaction loads computed with constraints to be at least three times more costly since the constrained system has three times the number of equations. We measured performance of the constrained system as 12 times slower, due primarily to the solution phase for Lagrange multipliers that enforce the ellipsoid constraint. That phase is skipped if there are no constraints. In a simulation, there are additional costs independent of the formulation so the overall speedup is lesser; in this case, we measured a factor of 10 with a constraint tolerance of 10^{-4}. The deviation from the permissible-motion manifold was essentially zero with the ellipsoid mobilizer while the constrained system error is maintained to the requested tolerance. With a tighter tolerance, the constrained system would run more slowly.

The simplicity of an ellipsoid mobilizer contrasts with the complexity of applying kinematic constraints to generate realistic motion of the shoulder. De Sapio et al. [48], for example, used nine generalized coordinates and five constraints to produce a 4-dof shoulder model.

2.4 General reversibility of a mobilizer

A tree of mobilized bodies is ordered parent-to-child along each branch in an internal coordinate formulation. It is therefore useful to reverse the topological direction of mobilizers while preserving the definition of the mobilities. For example, in the shoulder

model (Fig. 3), it is typical to have the thorax as the parent and the scapula and arm as descendants in a model of arm-reaching tasks. However, when modeling a push-up task with the hand affixed to ground, we can avoid constraints at the hand if the topology is reversed. However, we wish to preserve the definition of the generalized coordinates and speeds such that they describe the motion of the scapula relative to the thorax. Several internal-coordinate mechanical codes ignore this problem while others have addressed it with a library of "reverse" joints [33]. Featherstone [46] solved the problem generally for a non-Euclidean spatial vector formulation [42,49]; however, the mobilizer formulation, which uses spatial notation comprised of ordinary Euclidean vectors [50], is also generally reversible, as we show here.

Given a mobilizer in a reversed topological sense than desired if defined from frame *B* in a parent body (e.g. thorax) to frame *P* in a child body (e.g. scapula), that is ${}^{B}X^{P}$, ${}^{B}\mathbf{H}^{P}$, ${}^{B}\dot{\mathbf{H}}^{P}$, and **N** (with time derivatives taken in parent *B)* as in the above thorax-to-scapula ellipsoid mobilizer, the reversibility problem can be distilled to formulating the mobilizer that yields ${}^{P}X^{B}$, ${}^{P}\mathbf{H}^{B}$, ${}^{P}\dot{\mathbf{H}}^{B}$ and **N** describing a parent (scapula) frame *P* to body (thorax) frame *B* mobilizer (with time derivatives taken in now-parent *P*) with internal coordinate and mobility definitions preserved as though the parent body had remained the thorax.

Since we want *q* and *u* to retain their original meanings, **N** must stay the same. The position transform is easily reversed, with

$$ {}^{P}X^{B}=\left({}^{B}X^{P}\right)^{-1}=\left({}^{P}R^{B}|-{}^{P}R^{B}\cdot{}^{B}p^{P}\right), \tag{15}$$

where ${}^{P}R^{B}=\left({}^{B}R^{P}\right)^{\mathrm{T}}$. However, the time derivatives are taken in different moving frames, so these quantities cannot be simply reversed and must account for the relative angular velocity between the frames. This leads to

$$ {}^{P}\mathbf{H}^{B}=-{}^{P}R^{B}\begin{pmatrix} {}^{B}\mathbf{H}^{P}_{\omega} \\ {}^{B}\mathbf{H}^{P}_{v}+{}^{B}p^{PB}_{\times}\mathbf{H}^{P}_{\omega} \end{pmatrix}, \tag{16}$$

where $p\times$ is the skew-symmetric matrix form of the cross product. (Note the spatial notation of "scalar" multiplication for the rotation matrix ${}^{P}R^{B}$, which distributes across the rows of the spatial vector as though it were arranged $\begin{bmatrix} R & 0 \\ 0 & R \end{bmatrix}$ as with a scalar.)

Time differentiation of ${}^{P}\mathbf{H}^{B}$ in *P* yields:

$$ {}^{P}\dot{\mathbf{H}}^{B}={}^{P}\omega^{B}_{\times}\cdot{}^{P}\mathbf{H}^{B}-{}^{P}R^{B}\begin{pmatrix} {}^{B}\dot{\mathbf{H}}^{P}_{\omega} \\ {}^{B}\dot{\mathbf{H}}^{P}_{v}+{}^{B}p^{PB}_{\times}\dot{\mathbf{H}}^{P}_{\omega}+{}^{B}v^{PB}_{\times}\mathbf{H}^{P}_{\omega} \end{pmatrix}. \tag{17}$$

Equations (15)–(17) describe any available mobilizer as being reversed so that the motion between bodies is parameterized with respect to the child body, although the topology remains parent-to-child. When a modeler requires a reverse mobilizer, Simbody automates the process by first using the definition of the mobilizer to describe the motion of the parent in the child and then applies (15)–(17) to maintain the definition of the mobilities but obtain the desired parent-to-child topology to build the multibody tree.

3 Generic joint motion without constraints

The formulation of the position transform, relative spatial velocity and acceleration, and kinematic coupling equations in (1)–(4) comprise the essence of the mobilizer. However, it is undesirable to require biological researchers to formulate these transforms, hinge matrices and their derivatives. This section describes a general function based mobilizer that is configurable by user-specified functions and automates the process of deriving the hinge matrix and its derivative.

To simplify the specifications required by the modeler, we assume that $\dot{q} = u$ (i.e., **N** is identity in (4)) although the mobilities u are not necessarily the components of the relative spatial velocity. The kinematic relationship is scleronomic (dependent only on coordinates, q); thus, velocity and acceleration relationships can be derived from the position relationship. This is a subset of all the kinematic constraints that can be embedded in a mobilizer; however, it represents the majority of joint models based on the geometry of structures from experimental measurements (e.g., MRI of articulating bones). Specifically, experimental measurements or knowledge of the joint geometry enable the modeler to write the position transform ${}^{P}X^{B}$ of a body with respect to its parent. This transform is a map from the coordinate space, q, to the spatial orientation and position. For example, consider a particle whose motion in space is known to travel on a manifold (a surface in three dimensions) that was obtained from imaging data (Fig. 5). In conventional terms, a constraint equation is necessary to eliminate a dof to restrict the motion to the manifold. The constraint provides a reaction force that is normal to the manifold surface (arrow in Fig. 5), acting at whatever point the particle may be on the manifold.

In contrast, a mobilizer can parameterize the motion of the particle in Cartesian space such that its motion cannot exist off the manifold. This is done by first describing the spatial transform in terms of just two coordinates, x and θ, whose derivatives are the mobilities of the joint.

To facilitate the description of the orientation and position transform of a rigid body in 3-space, we write the spatial transform in terms of three rotational and three translational spatial coordinates, in θ and p:

$$
{}^{P}\mathbf{X}^{B}(\theta, p) = \begin{bmatrix} & & p_1 \\ & {}^{P}\mathbf{R}^{B}(\theta_1, \theta_2, \theta_3) & p_2 \\ & & p_3 \end{bmatrix}, \quad \text{where}
$$

$$
\begin{Bmatrix} \theta(q) \\ p(q) \end{Bmatrix} = \begin{Bmatrix} \theta_1(q_1, q_2, \ldots, q_m) \\ \theta_2(q_1, q_2, \ldots, q_m) \\ \theta_3(q_1, q_2, \ldots, q_m) \\ p_1(q_1, q_2, \ldots, q_m) \\ p_2(q_1, q_2, \ldots, q_m) \\ p_3(q_1, q_2, \ldots, q_m) \end{Bmatrix} \tag{18}
$$

that define a body-fixed Euler angle sequence (θ_1–θ_3) for the orientation and the components of the position (p_1–p_3) of the body in the parent. In turn, θ and p are functions of a set of m(1-6) mobilizer coordinates, q. We can now express the velocity of the body in terms of the underlying mobilities of the joint (since $\dot{q} = u$) given that θ and p are continuous and twice differentiable, with respect to q. Simbody automatically generates both ${}^{P}\mathbf{H}^{B}$ and ${}^{P}\dot{\mathbf{H}}^{B}$ to characterize the velocity and acceleration transformation enabled by this mobilizer.

We begin with the mobilizer's relative spatial velocity transformation with $\dot{q} = u$:

$$ {}^{P}V^{B} \equiv \left\{ \begin{array}{c} {}^{P}\omega^{B}(q,u) \\ {}^{P}v^{B}(q,u) \end{array} \right\} = {}^{P}\mathbf{H}^{B}(q)\, u = {}^{P}\mathbf{H}^{B}(q)\, \dot{q} \,. \tag{19} $$

Given that θ_1–θ_3 are rotations about body fixed axes ($\hat{a}_1$ to $\hat{a}_3$) that specify the rotation, ${}^{P}\mathbf{R}^{B}$, then

$$ {}^{P}\omega^{B} = \left[\begin{array}{ccc} \widehat{a}_1 & {}^{P}\mathbf{R}^{1}(\theta_1)\widehat{a}_2 & {}^{P}\mathbf{R}^{1}(\theta_1)\,{}^{1}\mathbf{R}^{2}(\theta_2)\widehat{a}_3 \end{array} \right] \left\{ \begin{array}{c} \dot{\theta}_1 \\ \dot{\theta}_2 \\ \dot{\theta}_3 \end{array} \right\} \tag{20} $$

is the relative angular velocity of the body in terms of the time derivatives of the Euler angles θ_1–θ_3, where ${}^{P}\mathbf{R}^{1}$ and ${}^{1}\mathbf{R}^{2}$ are the first and second body-fixed rotations. We can then define a transformation matrix, $\mathbf{W}$, from spatial speeds to relative angular velocity. The spatial (rotational) speeds are now expressed in terms of the mobilities according to the Jacobian, $\boldsymbol{\theta}_q$, of the rotational coordinate functions, θ, with respect to the mobilizer coordinates, q:

$$ {}^{P}\omega^{B} = \mathbf{W}\left[\frac{\partial \theta}{\partial q}\right]\dot{q} = \mathbf{W}\theta_q\,\dot{q} \tag{21} $$

which yields the transformation from the mobilities to the angular velocity of frame B in P:

$$ {}^{P}\mathbf{H}^{B}_{\omega} = \mathbf{W}\theta_q, \quad \text{where} \quad {}^{P}\mathbf{H}^{B} = \left[\begin{array}{c} {}^{P}\mathbf{H}^{B}_{\omega} \\ {}^{P}\mathbf{H}^{B}_{v} \end{array} \right]. \tag{22} $$

Similarly, given p_1–p_3 as the body translations along independent axes ($\hat{a}_4$ to $\hat{a}_6$) defined in the parent, we can express the velocity of the body in terms of the mobilities according to:

$$ {}^{P}v^{B} = \left[\begin{array}{ccc} \widehat{a}_4 & \widehat{a}_5 & \widehat{a}_6 \end{array} \right]\left[\frac{\partial p}{\partial q}\right]\dot{q}, \tag{23} $$

$$ {}^{P}v^{B} = \mathbf{A}\mathbf{p}_q\,\dot{q} \tag{24} $$

$$ \Rightarrow \quad {}^{P}\mathbf{H}^{B}_{v} = \mathbf{A}\mathbf{p}_q. \tag{25} $$

To obtain ${}^{P}\dot{\mathbf{H}}^{B}$, we differentiate the angular velocity to yield the angular acceleration β of B (the body) with respect to its parent:

$$ {}^{P}\beta^{B} = \frac{d}{dt}\left(\mathbf{W}\theta_q\,\dot{q}\right), \tag{26} $$

$$ {}^{P}\beta^{B} = \dot{\mathbf{W}}\,\theta_q\,\dot{q} + \mathbf{W}\frac{d}{dt}\left(\theta_q\,\dot{q}\right). \tag{27} $$

The time derivative of $\mathbf{W}$, in turn, is obtained from the fact that the body-fixed axes are rotating:

$$\dot{\mathbf{W}} = \begin{bmatrix} 0 & {}^{P}\omega_1^B \times W_2 & {}^{P}\omega_{1,2}^B \times W_3 \end{bmatrix}, \tag{28}$$

where ${}^{P}\omega_1^B$ and ${}^{P}\omega_{1,2}^B$ are the angular velocity vectors due to only the first and the first and second rotational speeds, respectively, and W_i is the corresponding column of **W**. The derivative of the transformation from mobilities to spatial speeds can be expanded:

$$\frac{d}{dt}\left(\theta_q\,\dot{q}\right) = \frac{d}{dq}\left(\theta_q\,\dot{q}\right)\dot{q} + \theta_q\ddot{q}, \tag{29}$$

where we define

$$\dot{\theta}_q = \frac{d}{dq}\left(\theta_q \cdot \dot{q}\right) = \begin{bmatrix} \sum_{i=1}^{m} \frac{\partial^2\theta_1}{\partial q_i \partial q_1}\dot{q}_i & \cdots & \sum_{i=1}^{m} \frac{\partial^2\theta_1}{\partial q_i \partial q_m}\dot{q}_i \\ \vdots & \ddots & \vdots \\ \sum_{i=1}^{m} \frac{\partial^2\theta_3}{\partial q_i \partial q_1}\dot{q}_i & \cdots & \sum_{i=1}^{m} \frac{\partial^2\theta_3}{\partial q_i \partial q_m}\dot{q}_i \end{bmatrix} \tag{30}$$

given that θ_i is twice differentiable to express the body angular acceleration in terms of the mobilities and their derivatives.

$${}^{P}\beta^B = \dot{\mathbf{W}}\,\theta_q\,\dot{q} + \mathbf{W}\left(\dot{\theta}_q\,\dot{q}\right) + \mathbf{W}\theta_q\ddot{q}, \tag{31}$$

$$= \left[\dot{\mathbf{W}}\,\theta_q + \mathbf{W}\dot{\theta}_q\right]\dot{q} + \mathbf{W}\theta_q\ddot{q}, \tag{32}$$

$$\Rightarrow \quad {}^{P}\dot{\mathbf{H}}_{\omega}^{B} = \left[\dot{\mathbf{W}}\,\theta_q + \mathbf{W}\dot{\theta}_q\right]. \tag{33}$$

The derivative of the translational velocity (where the axes, **A**, are constant) yields the translational acceleration of the body in the parent:

$${}^{P}a^B = \mathbf{A}\dot{\mathbf{p}}_q\,\dot{q} + \mathbf{A}\mathbf{p}_q\ddot{q} \tag{34}$$

$$\Rightarrow \quad {}^{P}\dot{\mathbf{H}}_{v}^{B} = \mathbf{A}\dot{\mathbf{p}}_q. \tag{35}$$

The automatic formulation of the position transform equation (18) and the hinge matrices equations (22), (25), (33), and (35) is implemented in Simbody, which creates a custom mobilizer based on user-supplied functions (θ and p) that can be either analytically defined or constructed as splines from user-specified data points, for example, those obtained from experimental measurements. This is a powerful tool for modeling unusual joints that are typical of biomechanisms.

4 Capturing the kinematics of the human knee

Mobilizers can be used to model the complex motion of the human knee. Unlike an ideal pin joint, the shape of the femoral condyles is not circular resulting in a non-stationary center of rotation [51,52]. Furthermore, both sliding and rolling of the femoral condyles on the tibial plateau surface (Fig. 6) lead to motion of the tibia with respect to the femur that includes translation in the plane of rotation. Biomechanists have characterized the translation of the

tibia based on experiments [51-53] and have created kinematic models that prescribe the translations of the tibia as spline functions of experimental data [35]. Recently, dynamical models of human gait [54-56] have allowed the tibia to move freely in the plane of rotation and then applied kinematic constraints to enforce the desired behavior of the knee based on Delp et al. [35].

Spline points from constraints in a knee model [35] were used to specify the functions of a custom mobilizer in Simbody, which couples the horizontal (x) and vertical (y) translations of the tibia (with respect to the femur) to a single knee-angle, θ (Fig. 6). The spline characterizes a permissible-motion manifold, which in this case is a curve in the unconstrained planar motion space of the tibia with respect to the femur as the knee flexes.

The spatial transform and hinge matrices for the resulting mobilizer, with $q = \theta$ and $u = \dot{\theta}$ such that both the single rotation and angular velocity of the tibia are about the z-axis of the femur's mobilizer frame (P in Fig. 6), are:

$$ {}^{P}\mathbf{X}^{B}(q) = \begin{bmatrix} {}^{P}\mathbf{R}^{B}(0,0,q) & \begin{matrix} f_x(q) \\ f_y(q) \\ 0 \end{matrix} \\ \end{bmatrix}, \tag{36} $$

$$ {}^{P}\mathbf{H}^{B}(q) = \begin{bmatrix} 0 & 0 & 1 & \frac{\partial f_x}{\partial q} & \frac{\partial f_y}{\partial q} & 0 \end{bmatrix}^{\mathrm{T}}, \tag{37} $$

$$ {}^{P}\dot{\mathbf{H}}^{B}\left(q,\dot{q}\right) = \begin{bmatrix} 0 & 0 & 0 & \frac{\partial^2 f_x}{\partial q^2}\dot{q} & \frac{\partial^2 f_y}{\partial q^2}\dot{q} & 0 \end{bmatrix}^{\mathrm{T}}, \tag{38} $$

$$ \mathbf{N} = 1. \tag{39} $$

These matrices (36)–(39) are created automatically; the user only supplies the empirical or analytical functions f_x and f_y mapping the knee-flexion angle to displacements.

The performance of the custom mobilizer implementation was compared to the application of constraints to enforce the coupled translations during knee-flexion. The calculation of the tibia acceleration and a leg swing simulation exercising the full range of motion were clocked and times were normalized by the time to perform the same evaluations using an ideal pin joint. The standard implementation required a planar joint with three dofs and two constraint equations for a system of five DAEs. Both the pin and custom mobilizer, on the other hand, required only one ODE but the custom mobilizer produced the physiologically relevant motion of the tibia, unlike the pin.

The calculation of the acceleration of the knee using the conventional approach of constraints required nearly six times more computing time than the custom mobilizer for the same results (Table 2). In terms of simulation cost (time to integrate the equations) the custom mobilizer implementation was 3.6 times faster than the use of constraints (in Simbody, version 1.5). Error tolerances for constraint violations were set to 10^{-4} (0.1 mm), which was also the same as the integration error tolerance. The custom mobilizer implementation, however, remained exactly (to machine precision) on the permissible-motion manifold using the same integration tolerance.

5 Capturing coarse-grained kinematics of proteins

Most molecular dynamics investigations are performed using atomistic simulations in which each atom is modeled as a point mass and bonds between them are modeled with forces [57]. A multibody treatment is unnecessary for simulating a system composed only of particles. However, it is common practice to constrain some of the bonds to remove the highest frequencies from a simulation and allow larger integration step sizes. When groups of atoms are treated as rigid bodies, multibody methods are appealing [24-27,29,58,59]. However, most molecular models group just a few atoms per body, and almost every torsion along an atomic bond is given a degree of freedom.

Large biomolecular machines are impractical to simulate in such detail and many are empirically observed to form nearly-rigid subcomponents, called domains, which move relative to one another. Domains may consist of hundreds or thousands of atoms. The connections among domains may exhibit very few degrees of freedom, but they are composed of numerous rotational bonds and are capable of complex coupled motions. Custom mobilizers simplify the dynamic model by incorporating empirical data to define the permissible-motion space of the model. The reduced model can then be used to perform coarse-grained simulations to investigate the large-scale dynamic behavior of macromolecules.

To illustrate this, we selected Lysine–Arginine–Ornithine (LAO) binding protein from the Hinge Atlas Gold (HAG) annotated set of domain hinge bending proteins [37,60]. According to the HAG annotation, the flexible hinge connecting the two domains consists of residues 90–91 and 192–193. The “mobile” domain (blue body in Fig. 7) is thus comprised of residues 92–191, while the remaining residues comprise the “stationary” domain (green).

To demonstrate how a mobilizer can be used to recreate bulk protein motion, a rigid-body model of the LAO protein consisting of two rigid bodies (one for each protein domain) connected by a custom hinge was constructed. In biomolecular parlance the molecule goes from an “open” state to a “closed” state; this does not represent a topological change. We first created a “synthetic-closed” conformation similar to the actual closed protein conformation by rotating and translating the mobile domain (as a rigid body) from the open conformation. We did this by structurally aligning the alpha-carbon atoms of the mobile domain of the open conformation to those of the closed conformation using Visual Molecular Dynamics [61]. The resultant mobile domain transformation specified by three Euler angles and three translation components was then parameterized by a single internal (mobilizer) coordinate, q, such that the mobile domain transitioned from the open to the closed conformation as a function of q (18) from 0 to 1. This single q is analogous to the reaction or transition coordinate in chemistry (International Union of Pure and Applied Chemistry). Note that we could have chosen two or more internal coordinates if desired to increase the modeled mobility.

Unlike purely kinematic models, however, the domains connected by the mobilizer are part of a multibody system in which forces can be applied to drive the conformational changes of the protein, as well as to estimate the net motive force necessary to generate observed motions. Likewise, reaction forces can be calculated to determine the bearing loads of the hinge region of the protein. Whether these models will yield information of biological importance has not been evaluated because practical methods to represent their motion and explore their dynamics have been unavailable.

Developing simulations across a range of physical scales may be enabled by these methods. For example, it may be possible to study the contractile behavior of muscle fibers (i.e. muscle cells) by first modeling the mechanics of myosin interacting with actin (e.g. [62])

with reduced coordinates and then to replicate thousands of these subunits to model the dynamics of a complete muscle fiber.

6 Discussion and conclusions

The mobilizer formulation encapsulates the mapping of the permissible spatial kinematics of a body with respect to its parent in terms of a reduced set of internal coordinates and speeds (i.e., the mobilities). This mapping (the hinge matrix, **H**) can vary as a function of the internal coordinates, which enables parameterization of a vast set of permissible-motion manifolds. The user-customizable mobilizer obviates the need for superfluous coordinates and the subsequent enforcement of scleronomic constraints to obtain a desired permissible-motion manifold for a joint. With fewer differential equations and no algebraic constraint equations to enforce, mobilizers improve the efficiency of simulating biomechanical joints. Since the mobilizer mapping is exact, no motion can exist off the manifold, and the accuracy of the solution is also improved. Fewer coordinates also facilitate optimization, such as fitting the model to an experimental trajectory by keeping the number of unknowns low and providing a smaller unconstrained solution space that is always on the desired manifold.

We have demonstrated new joints that can be formulated directly, such as the ellipsoid mobilizer, that provide novel behavior with no additional costs when compared to conventional joints with the same degrees of freedom, such as a ball-and-socket joint, but can be an order of magnitude faster than conventional joints with constraints. Furthermore, we have constructed a mobilizer that utilizes user-defined functions to automatically specify the position transform and hinge matrices when functions are twice differentiable and continuous with respect to the mobilizer coordinates. The improved accuracy of joint kinematics via the mobilizer, unlike the alternative of adding constraints, comes at low computational cost even when evaluating user-supplied functions. For a model of the human knee, simulations were 3.5 times faster for the mobilizer with embedded bone translation information than enforcing the same joint kinematics via constraints. The ability to embed joint-specific geometry from experimental measurements, such as MRI images of the human knee or known protein conformations from crystal structures, makes mobilizers practical for biomechanists and biomolecular modelers.

The mobilizer formulation improves the efficiency of internal-coordinate multibody dynamics and simplifies the specification of joints necessary to simulate biomechanisms. Speed and accuracy are garnered by minimizing the number of coordinates and eliminating joint constraints, thereby reducing the number of system equations. These are the benefits long enjoyed by mechanical engineers employing the state-of-the-art multibody formulations. Now the power of these methods can be enjoyed by biomechanists and computational biologists as well.

Acknowledgments

The authors are grateful to Samuel Flores and Christopher Bruns for their assistance with the molecular modeling example. This work was supported by the National Institute of Health, through the NIH Roadmap for Medical Research Grant U54 GM072970.

References

1. Hurwitz DE, Ryals AR, Block JA, Sharma L, Schnitzer TJ, Andriacchi TP. Knee pain and joint loading in subjects with osteoarthritis of the knee. J. Orthop. Res. 2000; 18(4):572–579. [PubMed: 11052493]

2. Baliunas AJ, Hurwitz DE, Ryals AB, Karrar A, Case JP, Block JA, Andriacchi TP. Increased knee joint loads during walking are present in subjects with knee osteoarthritis. Osteoarthr. Cartil. 2002; 10(7):573–579. [PubMed: 12127838]
3. Piazza SJ, Delp SL. Three-dimensional dynamic simulation of total knee replacement motion during a step-up task. J. Biomech. Eng. 2001; 123(6):599–606. [PubMed: 11783731]
4. Isralewitz B, Gao M, Schulten K. Steered molecular dynamics and mechanical functions of proteins. Curr. Opin. Struct. Biol. 2001; 11(2):224–230. [PubMed: 11297932]
5. Tang S, Liao J-C, Dunn AR, Altman RB, Spudich JA, Schmidt JP. Predicting allosteric communication in myosin via a pathway of conserved residues. J. Mol. Biol. 2007; 373(5):1361–1373. [PubMed: 17900617]
6. Sponer, J.; Lankas, F., editors. Computational Studies of RNA and DNA. Springer; Berlin: 2006.
7. Kitano H. Systems biology: A brief overview. Science. 2002; 295(5560):1662–1664. [PubMed: 11872829]
8. Kuhlman B, Dantas G, Ireton GC, Varani G, Stoddard BL, Baker D. Design of a novel globular protein fold with atomic-level accuracy. Science. 2003; 302(5649):1364–1368. [PubMed: 14631033]
9. Eich-Soellner, E.; Fuhrer, C. Numerical Methods in Multibody Dynamics. Tuebner; Leipzig: 1998.
10. Kane, TR.; Likins, PW.; Levinson, DA. Spacecraft Dynamics. McGraw-Hill; New York: 1983.
11. Jain A. Unified formulation of dynamics for serial rigid multibody systems. J. Guid. Control Dyn. 1991; 14:531–542.
12. Brenan, K.; Campbell, S.; Petzold, LR. Numerical Solution of Initial-Value Problems in Differential-Algebraic Equations. 2nd edn.. SIAM; Philadelphia: 1987.
13. Baumgarte J. Stabilization of constraints and integrals of motion in dynamic systems. Comput. Methods Appl. Mech. Eng. 1972; 1:1–16.
14. Eich E. Convergence results for a coordinate projection method applied to mechanical systems with algebraic constraints. SIAM J. Numer. Anal. 1993; 30(5):1467–1482.
15. Sobieszczanski-Sobieski J, Haftka RT. Multidisciplinary aerospace design optimization: Survey of recent developments. Struct. Multidiscip. Optim. 1997; 14(1):1–23.
16. Reinbolt J, Schutte J, Fregly B, Koh B, Haftka R, George A, Mitchell K. Determination of patient-specific multi-joint kinematic models through two-level optimization. J. Biomech. 2005; 38(3): 621–626. [PubMed: 15652563]
17. Anderson KS, Hsu Y. Analytical fully-recursive sensitivity analysis for multibody dynamic chain systems. Multibody Syst. Dyn. 2002; 8(1):1–27.
18. Stryk O. Optimal control of multibody systems in minimal coordinates. ZAMM-Z. Angew. Math. Mech. 1998; 78:1117–1120.
19. Lo, J.; Metaxas, D. Recursive dynamics and optimal conrol techniques for human motion planning; Computer Animation Proceedings; Geneva, Switzerland. 1999; p. 220-234.
20. Neptune RR, Hull ML. Evaluation of performance criteria for simulation of submaximal steady-state cycling using a forward dynamic model. J. Biomech. Eng. 1998; 120(3):334–341. [PubMed: 10412400]
21. Anderson F, Pandy M. A dynamic optimization solution for vertical jumping in three dimensions. Comput. Methods Biomech. Biomed. Eng. 1999; 2(3):201–231.
22. Delp S, Loan J. A computational framework for simulating and analyzing human and animal movement. Comput. Sci. Eng. 2000; 2(5):46–55.
23. McLean SG, Su A, van den Bogert AJ. Development and validation of a 3-D model to predict knee joint loading during dynamic movement. J. Biomech. Eng. 2003; 125(6):864–874. [PubMed: 14986412]
24. Brunger A, Adams P, Clore G, DeLano W, Gros P, Grosse-Kunstleve R, Jiang J, Kuszewski J, Nilges M, Pannu N. Crystallography & NMR system: A new software suite for macromolecular structure determination. Acta Crystallogr. D Biol. Crystallogr. 1998; 54(5):4449.
25. Schwieters CD, Clore GM. Internal coordinates for molecular dynamics and minimization in structure determination and refinement. J. Magn. Reson. 2001; 152(2):288–302. [PubMed: 11567582]

26. Guntert P, Mumenthaler C, Wuthrich K. Torsion angle dynamics for NMR structure calculation with the new program Dyana. J. Mol. Biol. 1997; 273:283. [PubMed: 9367762]
27. Vaidehi N, Jain A, Goddard W III. Constant temperature constrained molecular dynamics: The Newton–Euler inverse mass operator method. J. Phys. Chem. 1996; 100(25):10508–10517.
28. Kalani MYS, Vaidehi N, Hall SE, Trabanino RJ, Freddolino PL, Kalani MA, Floriano WB, Kam VWT, Goddard WA. The predicted 3D structure of the human D2 dopamine receptor and the binding site and binding affinities for agonists and antagonists. Proc. Natl. Acad. Sci. USA. 2004; 101(11):3815–3820. [PubMed: 14999101]
29. Tóth G, Borics A. Flap opening mechanism of HIV-1 protease. J. Mol. Graph. 2006; 24(6):465–474.
30. Featherstone, R. Robot Dynamics Algorithms. Kluwer; Amsterdam: 1987.
31. Rodriguez G, Jain A, Kreutz-Delgado K. Spatial operator algebra for multibody system dynamics. J. Astronaut. Sci. 1992; 44(1):27–50.
32. Anderson K, Critchley J. Improved 'Order-N' performance algorithm for the simulation of constrained multirigid-body dynamic systems. Multibody Syst. Dyn. 2003; 9(2):185–212.
33. Hollars, MG.; Rosenthal, DE.; Sherman, MA. SD/FAST User's, Guide B.2. 1994.
34. The Mathworks. Simmechanics 3 reference. October. 2008
35. Delp SL, Loan JP, Hoy MG, Zajac FE, Topp EL, Rosen JM. An interactive graphics-based model of the lower extremity to study orthopaedic surgical procedures. IEEE Trans. Biomed. Eng. 1990; 37(8):757–767. [PubMed: 2210784]
36. van der Helm FCT. Analysis of the kinematic and dynamic behavior of the shoulder mechanism. J. Biomech. 1994; 27(5):527–550. [PubMed: 8027089]
37. Krebs WG, Gerstein M. Survey and summary: The morph server: A standardized system for analyzing and visualizing macromolecular motions in a database framework. Nucleic Acids Res. 2000; 28(8):1665–1675. [PubMed: 10734184]
38. Lee S-H, Terzopoulos D. Spline joints for multibody dynamics. ACM Trans. Graph. 2008; 27(3): 1–8.
39. Jain A, Vaidehi N, Rodriguez G. A fast recursive algorithm for molecular dynamics simulation. J. Comput. Phys. 1993; 106(2):258–268.
40. Kwatny HG, Blankenship GL. Symbolic construction of models for multibody dynamics. IEEE Trans. Robot. Autom. 1995; 11(2):271–281.
41. Mukherjee R, Anderson K. Orthogonal complement based divide-and-conquer algorithm for constrained multibody systems. Nonlinear Dyn. 2007; 48(1):199–215.
42. Featherstone R. The calculation of robot dynamics using articulated-body inertias. Int. J. Robot. Res. 1983; 2(1):13–30.
43. Schmidt JP, Delp SL, Sherman MA, Taylor CA, Pande VS, Altman RB. The Simbios National Center: Systems biology in motion. Proc. IEEE. 2008; 96(8):1266–1280.
44. Ryan, R. Adams-multibody system analysis software. In: Schiehlen, W., editor. Multibody Systems Handbook. Springer; Berlin: 1990.
45. Fritzson, P. Principles of Object-Oriented Modeling and Simulation with Modelica 2.1. IEEE; New York: 2004.
46. Featherstone, R. Rigid Body Dynamics Algorithms. 2nd edn.. Springer; Berlin: 2008.
47. Gu D, Chen Y, Dai K, Zhang S, Yuan J. The shape of the acetabular cartilage surface: A geometric morphometric study using three-dimensional scanning. Med. Eng. Phys. 2008; 30(8):1024–1031. [PubMed: 18276182]
48. De Sapio, V.; Holzbaur, K.; Khatib, O. The control of kinematically constrained shoulder complexes: Physiological and humanoid examples; Proceedings of the IEEE International Conference on Robotics and Automation; Orlando, FL. IEEE, New York. 2006; p. 2952-2959.
49. Featherstone, R. Plucker basis vectors; Proceedings of the IEEE International Conference on Robotics and Automation; Orlando, FL. IEEE, New York. 2006; p. 1892-1897.
50. Rodriguez G. Kalman filtering, smoothing, and recursive robot arm forward and inverse dynamics. IEEE J. Robot. Autom. 1987; 3(6):624–639.

51. Yamaguchi GT, Zajac FE. A planar model of the knee joint to characterize the knee extensor mechanism. J. Biomech. 1989; 22(1):1–10. [PubMed: 2914967]
52. Wilson D, Feikes J, Zavatsky A, O'Connor J. The components of passive knee movement are coupled to flexion angle. J. Biomech. 2000; 33(4):465–473. [PubMed: 10768395]
53. Dennis DA, Komistek RD, Ho WA, Gabriel SM. In vivo knee kinematics derived using an inverse perspective technique. Clin. Orthop. Relat. Res. 1996; 331:107–117. [PubMed: 8895626]
54. Thelen D, Anderson F. Using computed muscle control to generate forward dynamic simulations of human walking from experimental data. J. Biomech. 2006; 39(6):1107–1115. [PubMed: 16023125]
55. Delp SL, Anderson FC, Arnold AS, Loan P, Habib A, John CT, Guendelman E, Thelen DG. OpenSim: Open-source software to create and analyze dynamic simulations of movement. IEEE Trans. Biomed. Eng. 2007; 54(11):1940–1950. [PubMed: 18018689]
56. Liu M, Anderson F, Schwartz M, Delp S. Muscle contributions to support and progression over a range of walking speeds. J. Biomech. 2008; 41(15):3243–3252. [PubMed: 18822415]
57. Leach, A. Molecular Modelling: Principles and Applications. Longman; New York: 1996.
58. Sonnenschein R. An improved algorithm for molecular dynamics simulation of rigid molecules. J. Comput. Phys. 1985; 59(2):347–350.
59. Chun HM, Padilla CE, Chin DN, Watanabe M, Karlov VI, Alper HE, Soosaar K, Blair KB, Becker OM, Caves LSD, Nagle R, Haney DN, Farmer BL. MBO(n)D: A multibody method for long-time molecular dynamics simulations. J. Comput. Chem. 2000; 21(3):159–184.
60. Flores SC, Keating KS, Painter J, Morcos F, Nguyen K, Merritt EA, Kuhn LA, Gerstein MB. Hingemaster: Normal mode hinge prediction approach and integration of complementary predictors. Proteins. 2008; 73(2):299–319. [PubMed: 18433058]
61. Humphrey W, Dalke A, Schulten K. VMD: Visual molecular dynamics. J. Mol. Graph. 1996; 14(1):33–38. [PubMed: 8744570]
62. Parker D, Bryant Z, Delp SL. Coarse-grained structural modeling of molecular motors using multibody dynamics. Cell. Mol. Bioeng. 2009; 2(3):366–374. [PubMed: 20428469]

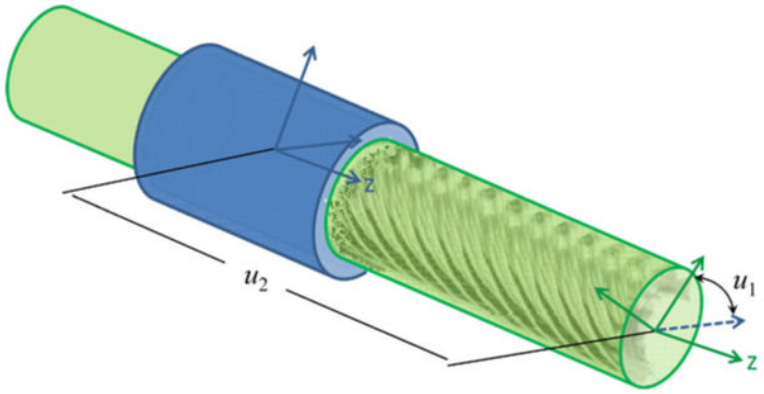

Fig. 1.
Screw motion. A collar body translates (u_2) along a common *z*-axis with a screw as it spins (u_1) about the same axis

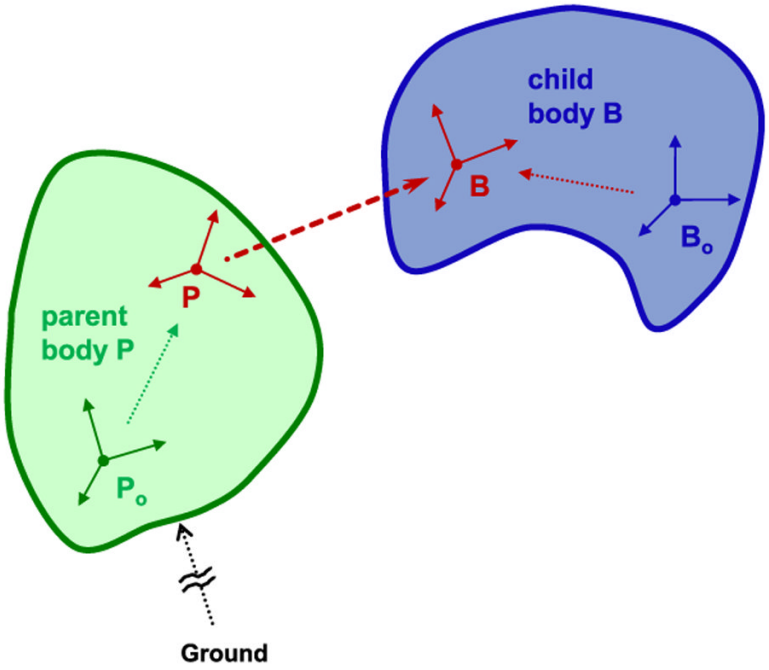

Fig. 2.

A mobilizer (*bold dashed arrow*) is the kinematic relationship between two bodies (a parent *P* and a child body *B*) parameterized by 1 to 6 mobilities in Euclidian space. Equations of motion are recursively generated in terms of the derivatives of the mobilities and applied forces of each body

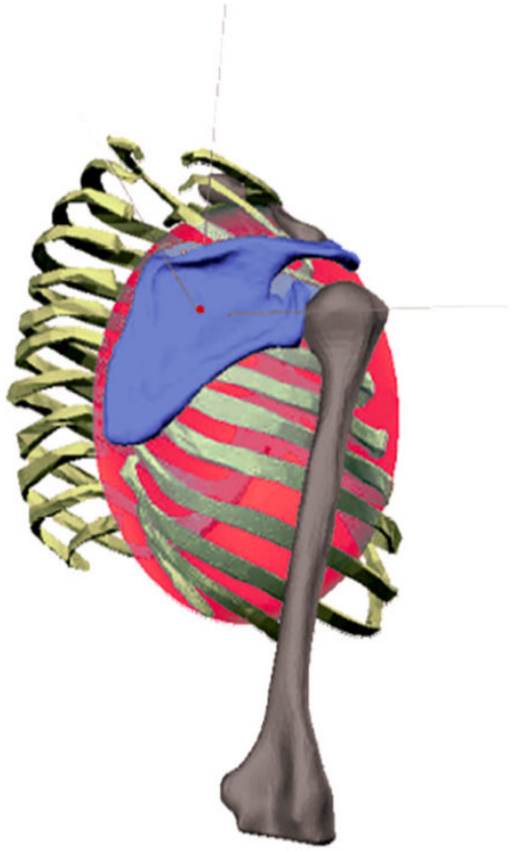

Fig. 3.
An ellipsoid mobilizer used to model the human shoulder. The scapula (*blue*) contacts the thorax approximated by an ellipsoid surface (*shaded red*) affixed to the ribs (*green*) at a point (axes' origin) in the scapula

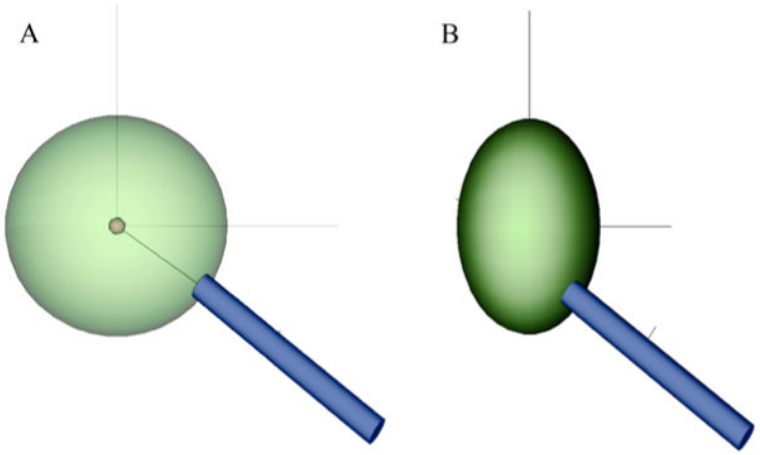

Fig. 4.

Ball-and-socket and ellipsoid mobilizers. A ball mobilizer (**A**) (drawn without the socket) enables the purely rotational motion of a body (*blue*) about the center of the ball. The ellipsoid mobilizer (**B**) requires the body to trace and remain normal to the surface of an ellipsoid

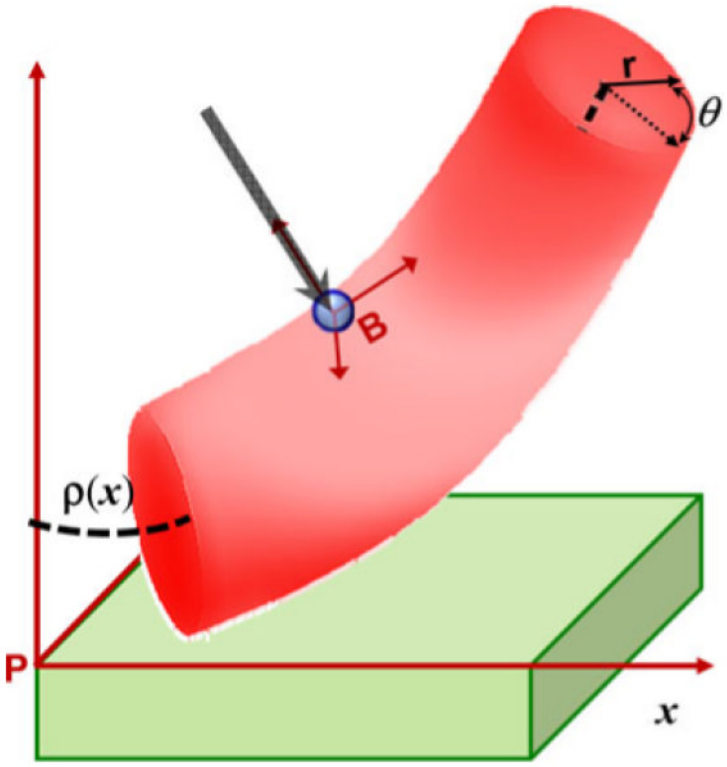

Fig. 5.
Example of a permissible-motion manifold. The manifold is a 2-dimensional surface in Cartesian space and is parameterized by two coordinates, x and θ, where ρ is a vector function of x and the radius of the manifold is a constant, r. The *arrow* illustrates the direction of the orthogonal reaction loads necessary to enforce motion of a particle along the permissible-motion manifold

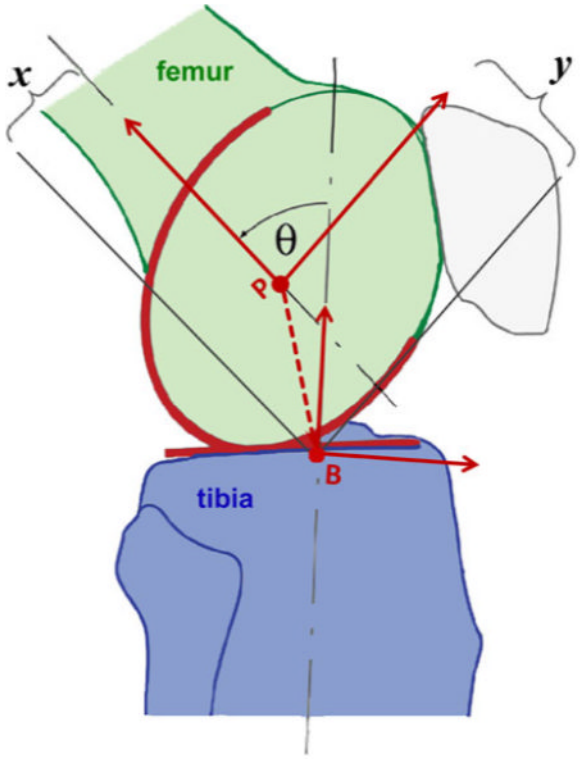

Fig. 6.

Schematic of the human knee joint (adapted from Delp et al. [35]). Due to the rolling and sliding of the non-circular femoral condyles (oval fixed in the femur, parent *P*) on the tibia plateau (body, *B*), the joint does not operate as a simple pin. In this model, the tibia has one rotational degree-of-freedom, θ, but translates in the plane of rotation (x, y) with respect to the femur

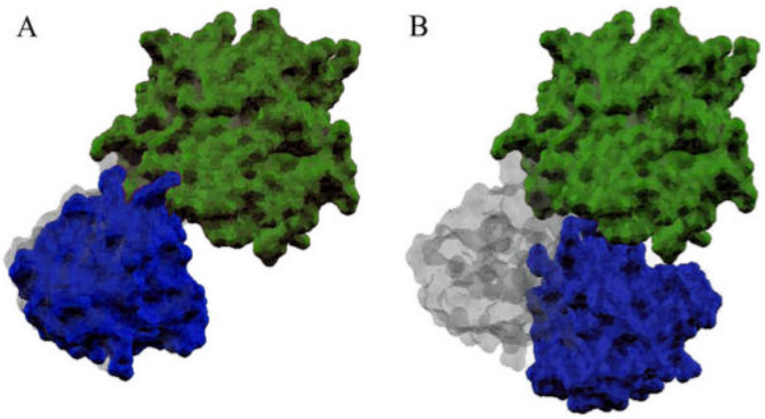

Fig. 7.
Simulated conformations of Lysine–Arginine–Ornithine (LAO) binding protein from (**A**) open ($q = 0$) to (**B**) closed ($q = 1$)

Table 1

Computational cost of the ellipsoid mobilizer versus a free joint with constraints. Computation times are normalized by the corresponding performance time for a ball mobilizer with identical initial conditions. The final row summarizes the relative speedup of the ellipsoid implementation versus constraints

Method	Acceleration compute time (× Ball time)	Simulation time (× Ball time)	Permissible-motion manifold error
Ellipsoid	0.98	1.01	$\sim 10^{-14}$
Constraints	11.84	10.37	$\sim 10^{-4}$
Speedup (×)	12.1	10.3	

Nonlinear Dyn. Author manuscript; available in PMC 2011 October 1.

Table 2

Performance of a custom mobilizer implementation of the human knee versus constraints. Computation times are normalized by the corresponding performance time for a pin joint. The final row summarizes the relative speedup factor of the implementation of a custom mobilizer versus constraints

Method	Acceleration compute time (× Pin Time)	Simulation time (× Pin Time)	Permissible-motion violation (mm)
Custom mobilizer	1.28	1.98	$\sim 10^{-11}$
Constraints	7.26	7.17	$\sim 10^{-1}$
Speedup (×)	5.7	3.6	